Continuum percolation for randomly oriented soft-core prisms

Martin O. Saar* and Michael Manga
Department of Earth and Planetary Science, University of California Berkeley, Berkeley, California 94720
(Received 24 January 2002; published 22 May 2002)

We study continuum percolation of three-dimensional randomly oriented soft-core polyhedra (prisms). The prisms are biaxial or triaxial and range in aspect ratio over six orders of magnitude. Results for prisms are compared with studies for ellipsoids, rods, ellipses, and polygons and differences are explained using the concept of the average excluded volume, $\langle v_{ex} \rangle$. For large-shape anisotropies we find close agreement between prisms and most of the above-mentioned shapes for the critical total average excluded volume, $n_c \langle v_{ex} \rangle$, where n_c is the critical number density of objects at the percolation threshold. In the extreme oblate and prolate limits simulations yield $n_c \langle v_{ex} \rangle \approx 2.3$ and $n_c \langle v_{ex} \rangle \approx 1.3$, respectively. Cubes exhibit the lowest-shape anisotropy of prisms minimizing the importance of randomness in orientation. As a result, the maximum prism value, $n_c \langle v_{ex} \rangle \approx 2.79$, is reached for cubes, a value close to $n_c \langle v_{ex} \rangle = 2.8$ for the most equant shape, a sphere. Similarly, cubes yield a maximum critical object volume fraction of $\phi_c = 0.22$. ϕ_c decreases for more prolate and oblate prisms and reaches a linear relationship with respect to aspect ratio for aspect ratios greater than about 50. Curves of ϕ_c as a function of aspect ratio for prisms and ellipsoids are offset at low-shape anisotropies but converge in the extreme oblate and prolate limits. The offset appears to be a function of the ratio of the normalized average excluded volume for ellipsoids over that for prisms, $R = \langle \overline{v_{ex}} \rangle_e / \langle \overline{v_{ex}} \rangle_p$. This ratio is at its minimum of $R = 0.758$ for spheres and cubes, where $\phi_{c(sphere)} = 0.2896$ may be related to $\phi_{c(cube)} = 0.22$ by $\phi_{c(cube)} = 1 - [1 - \phi_{c(sphere)}]^R = 0.23$. With respect to biaxial prisms, triaxial prisms show increased normalized average excluded volumes, $\langle \overline{v_{ex}} \rangle$, due to increased shape anisotropies, resulting in reduced values of ϕ_c. We confirm that $B_c = n_c \langle v_{ex} \rangle = 2C_c$ applies to prisms, where B_c and C_c are the average number of bonds per object and average number of connections per object, respectively.

DOI: 10.1103/PhysRevE.65.056131 PACS number(s): 64.60.Ak, 68.35.Rh, 05.10.Ln

I. INTRODUCTION

The transport properties of multiphase materials may either reflect the deformation of the material as a whole under applied stress (rheology) or the transfer of some medium, such as electrons or fluids, within the material (conductivity). Both types of transport are fundamentally different and depend on the relevant material properties in different ways. However, rheology and conductivity of composite materials are both determined in part by the interconnectivity of their individual elements (objects) that constitute their phases.

Percolation theory describes interconnectivity of objects in a random multiphase system as a function of the geometry, distribution, volume fraction, and orientation of the objects. The structure of the composite material may evolve with time due to chemical reactions or temperature changes. A critical threshold may be passed during the structural evolution and as a result some material properties such as yield strength or conductivity can change abruptly and may exhibit a power-law behavior above, and close to, the so-called percolation threshold.

Examples of composite materials that show time-dependent rheology include cements [1], gels [2], and magmas [3]. Similarly, the conductivity of a medium for fluids (permeability) or electrons may change with time. For example the permeability of a material changes with the formation or closure of pores and fractures in solids [4] or with growth and coalescence or degassing of bubbles in liquids [5]. Similarly, electrical conductivity depends on the amount, geometry, and interconnectivity of the conductor [6–8]. In general, multiple processes [9] in the physical, chemical, biological, and earth sciences appear to show power law, i.e., fractal, properties above a certain threshold and may thus be described by percolation theory.

Several soft-core (interpenetrating objects) continuum (randomly positioned) percolation studies have been conducted in three-dimensional (3D) systems. Investigated 3D percolating objects include spheres [10–13], parallel-aligned [6] or randomly oriented [14] ellipsoids, parallel-aligned cubes [6], and randomly oriented hemispherically capped cylinders [15,16]. In some studies, randomly oriented 2D ellipses [17] and 2D polygons [4] are placed in a 3D system to simulate fractures where the third object dimension may be neglected.

In this paper we investigate continuum percolation for randomly oriented 3D soft-core prisms. The objective is to point out similarities between prisms and other percolation systems studied previously, to expand on explanations for differences using the excluded volume concept [18] as introduced by Balberg *et al.* [16,19], and to compare the number of bonds per object to the total average excluded volume [16]. The latter two parameters may serve as ''quasi''-invariants [16,19,20]. We investigate prisms because in a 3D system, results can be compared in the extreme oblate limit with 2D polygons and 2D ellipses, in the extreme prolate limit with hemispherically capped cylinders or rods, and for all aspect ratios with ellipsoids. Furthermore, our paper is motivated by the observation that some media, such as sus-

*Email address: saar@seismo.berkeley.edu; http://seismo.berkeley.edu/~saar

pensions containing prismatic particles that can intergrow (e.g., crystal-melt suspensions, such as some magmas [3]) may best be described by interpenetrating 3D polyhedra.

Parameters of interest at the percolation threshold are the critical number density of prisms n_c, the critical prism volume fraction ϕ_c, and the critical total average excluded volume $\langle V_{ex}\rangle$. The latter parameter is given by $\langle V_{ex}\rangle \equiv n_c\langle v_{ex}\rangle$ [16], where the excluded volume v_{ex} is the volume around an object in which the center of another such object cannot be placed without overlap [18]. The angular brackets, $\langle\rangle$, denote spatial averaging over all orientation (and size) distributions. We determine numerically the average excluded volume, $\langle v_{ex}\rangle$, for some prism shapes. Finally, the critical average number of bonds per object, B_c, is determined numerically and compared with $\langle V_{ex}\rangle$. All parameters are investigated for possible contributions to an invariant allowing predictions of percolation thresholds. Because of the sometimes misleading nomenclature, especially concerning B_c, we review some percolation theory concepts throughout this paper.

II. METHOD

In a soft-core system the percolation threshold is reached when a continuous pathway of overlapping objects exists connecting opposing sides of a bounding box. Our computer code determines the percolation threshold and related parameters for convex 3D soft-core polyhedra of any shape, size, and orientation distribution that are randomly positioned (continuum percolation). Here we focus on randomly oriented biaxial and triaxial soft-core prisms of uniform size. In soft-core continuum percolation, size distribution of objects does not appear to affect ϕ_c [3] and results for parallel-aligned objects are independent of object shape [19].

Overlap of objects is determined analytically. The volume fraction of a phase is determined by the number density of objects n that constitute the phase and the object's unit volume V by [21]

$$\phi = 1 - \exp(-nV). \tag{1}$$

Results for ϕ using Eq. (1) can be verified through comparison with numerical volume fraction calculations using a space discretization method [3]. In order to reduce finite size effects and the possibility of imposing large-scale structure we place objects within a large unit bounding box whose volume typically is 8 to 64 times larger than the volume of an inner bounding box used to determine connection between opposing sides (Fig. 1). The more common approach is to perform calculations with periodic boundary conditions [4,14,17]. In all simulations, the largest object side length is one tenth or less of the side length of the inner bounding box. Figure 1 shows visualizations of simplified simulations for randomly oriented biaxial oblate and prolate prisms.

Our computational method is tested by comparing results with well-established values, such as ϕ_c and $\langle v_{ex}\rangle$ for spheres and parallel-aligned objects [6,16], and by visualizations of simulations at low n_c. Moreover, the critical number density of clusters per unit volume n_{sc} at percolation scales as $n_{sc} \propto s^{-\tau}$ over more than four orders of magnitude of s, where s is the number of objects in a cluster and $\tau \approx 2.2$. Thus, the cluster-size distribution follows the power-law relationship expected between n_{sc} and s close to the percolation threshold [22,23], suggesting that finite-size effects are minimal.

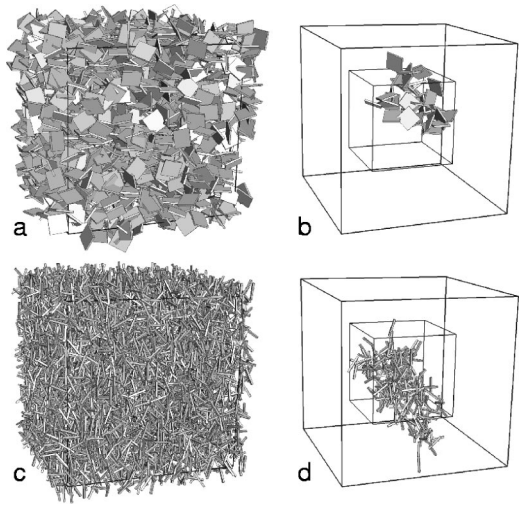

FIG. 1. Visualization of a *simplified* simulation of large biaxial oblate (a) and (b) and prolate (c) and (d) prisms with aspect ratios 1:10 (short-over-long axis) and 10:1 (long-over-short axis), respectively. The critical number densities are $n_c = 1060$ and $n_c = 7025$ for the oblate and prolate prism simulations, respectively. In *actual* simulations object side lengths are about 1/10 or less than the side length of the inner bounding box. n_c increases with object elongation up to $n_c = 7 \times 10^5$ for prolate prisms of aspect ratio 1000:1. The inner bounding box is used to determine if a continuous phase, or backbone (b) and (d) exists (percolation threshold). Objects are placed throughout the inner and outer bounding box and within a fringe around the outer box so that objects can protrude into the box (a) and (c). The average number of bonds per object B_c and the number density n_c are determined using all object overlaps and object centers, respectively, that fall within the large bounding box.

For two continuous convex objects the average excluded volume $\langle v_{ex}\rangle$ can be determined analytically by

$$\langle v_{ex}\rangle = V_a + V_b + (A_a R_a + A_b R_b)/4\pi, \tag{2}$$

where V is the volume, A the area, and R the mean radius of curvature of the objects a and b [24]. The prisms in this study, however, have corners so that R, and thus $\langle v_{ex}\rangle$, cannot be determined analytically using Eq. (2). Instead we employ a method analogous to Garboczi *et al.* [14] and de la Torre *et al.* [25], and determine $\langle v_{ex}\rangle$ numerically by randomly placing two objects of random orientation within a box and testing for overlap. This is repeated typically 10^6 times and the ratio of the number of overlaps over the total number of trials times the volume of the box is $\langle v_{ex}\rangle$. To obtain a mean and a standard error, we repeat the above procedure ten times. We test this method for the case of parallel-aligned objects of volume V, where in 3D for any convex object shape $\langle v_{ex}\rangle = 8 \times V$. This is also a test of the contact function for objects [14].

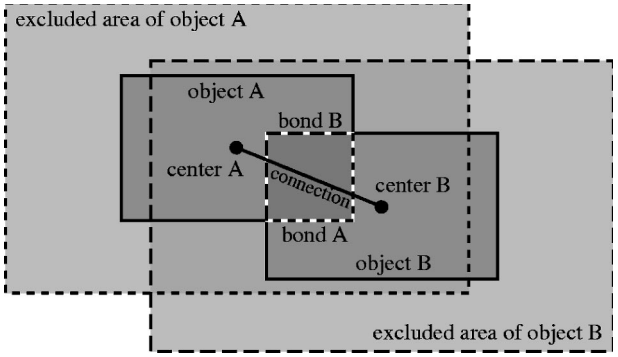

FIG. 2. Illustration of the overlap of two objects in a 2D parallel-aligned system (for easier visualization). The center of each object A and B falls within the other object's excluded area, each resulting in an overlap, or bond. The number of bonds is 2. In contrast, the number of connections per object is the total number of bonds (2) divided by the total number of objects (2), here resulting in one connection. In our 3D system, randomly oriented objects have average excluded volumes, rather than excluded areas.

All simulations are repeated ten times to calculate a mean and its standard error for ϕ_c, n_c, and B_c. Error bars in all figures indicate 95% confidence intervals. Biaxial object aspect ratios are given as small-over-large and as large-over-small axis length for oblate and prolate objects, respectively. The shape anisotropy ξ of an object is defined here as the ratio of large-over-short axis length for both oblate and prolate objects.

III. AVERAGE NUMBER OF BONDS PER OBJECT B_c

Objects in soft-core continuum percolation can interpenetrate each other. The average excluded volume $\langle v_{ex}\rangle$ is always defined for two objects (A and B). When placed within a unit volume $\langle v_{ex}\rangle$ describes the probability of each center A and B being within the other object's excluded volume, each causing an overlap, or bond (Fig. 2).

Therefore, in a unit volume, $n\langle v_{ex}\rangle$ describes the probability of n object centers being within n excluded volumes each causing an overlap, or bond, for each individual object, or two bonds per connection (Fig. 2). This method of counting each bond is commonly referred to as counting ''bonds per object,'' which has to be distinguished from the more intuitive average number of connections per object

$$C=\frac{(\text{total number of bonds})}{(\text{total number of objects})}, \tag{3}$$

denoted C_c at percolation. The critical average number of bonds per object at percolation is given by [16]

$$B_c=n_c\langle v_{ex}\rangle \tag{4}$$

and thus [26]

$$C_c=\frac{n_c\langle v_{ex}\rangle}{2}=\frac{B_c}{2}. \tag{5}$$

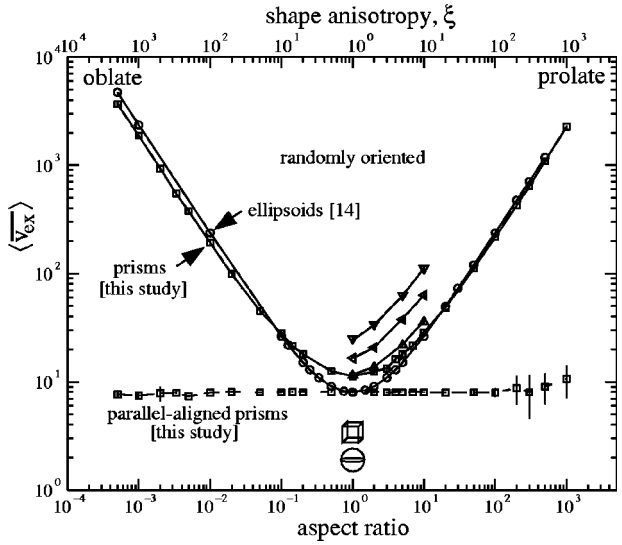

FIG. 3. Normalized average excluded volume $\langle\overline{v_{ex}}\rangle$ as a function of object aspect ratio (and shape anisotropy, ξ) for biaxial (squares) and triaxial (triangles) prisms (this study) and rotational (biaxial) ellipsoids (circles, from [14]). Solid and dashed lines indicate random and parallel orientation, respectively. Error bars for prisms indicate 95% confidence intervals. Short-over-medium axis aspect ratios for triaxial prisms are 1/2 (upward-pointing triangle), 1/5 (leftward-pointing triangle), and 1/10 (downward-pointing triangle). Long-over-medium axis aspect ratios are as indicated by the figure axis. $\langle\overline{v_{ex}}\rangle$ is calculated using B_c and n_c in Eq. (4) for randomly oriented prisms (squares along solid line). Squares along the dashed line show $\langle\overline{v_{ex}}\rangle$ for parallel-aligned biaxial prisms, determined using the method described in Sec. II.

For example, $B_c=1.4$ indicates a 140% probability per object to have a bond, or on average each object has 1.4 bonds, or 0.70 connections.

We determine B_c (and thus C_c), n_c, and $\langle v_{ex}\rangle$ numerically and can thus confirm Eqs. (4) and (5) for randomly oriented prisms. For example, for an aspect ratio of 3:1 we obtain $\langle\overline{v_{ex}}\rangle=\langle v_{ex}\rangle/V=13.1$ and $\langle\overline{v_{ex}}\rangle=B_c/(n_cV)=13.3$. Hereafter, we use Eq. (4) to calculate $\langle v_{ex}\rangle$ from B_c and n_c for randomly oriented prisms. In general, the larger number of overlaps in our simulation results in a more rapid and accurate estimate of $\langle v_{ex}\rangle$ using Eq. (4) than the method described in Sec. II.

IV. NORMALIZED AVERAGE EXCLUDED VOLUME $\langle\overline{V_{ex}}\rangle$

The normalized average excluded volume

$$\langle\overline{v_{ex}}\rangle=\langle v_{ex}\rangle/V \tag{6}$$

is the factor by which the excluded volume is larger than the actual volume V of an object. Figure 3 shows $\langle\overline{v_{ex}}\rangle$ as a function of aspect ratio for randomly oriented (solid line) biaxial (squares) and triaxial (triangles) prisms and for parallel-aligned biaxial prisms (squares along dashed line).

As indicated in Sec. II, $\langle\overline{v_{ex}}\rangle=8$ for any parallel-aligned convex 3D object. In contrast, randomly oriented biaxial prisms exhibit an increase in $\langle\overline{v_{ex}}\rangle$ with increasing shape

anisotropy ξ due to flattening or elongation. The combined effect of three different axis lengths of randomly oriented triaxial prisms increases $\langle \overline{v_{ex}} \rangle$ further. This dependency of $\langle \overline{v_{ex}} \rangle$ on shape anisotropy is expected because randomly oriented objects with eccentric shapes have a higher probability to overlap than objects of more equant shapes. In the extreme oblate and prolate limits the exponents in the power-law between aspect ratio and $\langle \overline{v_{ex}} \rangle$ are close to ± 1 (Fig. 3) indicating a linear relationship.

Also shown in Fig. 3 (circles) is the normalized average excluded volume $\langle \overline{v_{ex}} \rangle_e$ for rotational ellipsoids from [14] recalculated from their data and Eq. (11) in [14]. Identical values are obtained for $\langle \overline{v_{ex}} \rangle_e$ when using data from [14] and employing Isihara's [24] original equation as formulated by Nichol *et al.* [27] and given here in our notation and with volume normalization as

$$\langle \overline{v_{ex}} \rangle_e = 2 + \frac{3}{2}\left(1 + \frac{\sin^{-1}\epsilon}{\epsilon\sqrt{1-\epsilon^2}}\right)\left(1 + \frac{1-\epsilon^2}{2\epsilon}\ln\frac{1+\epsilon}{1-\epsilon}\right), \quad (7)$$

where the eccentricity $\epsilon^2 = 1 - b^2/a^2$ is given for prolate and oblate ellipsoids with long axis a and short axis b.

V. CRITICAL TOTAL AVERAGE EXCLUDED VOLUME $\langle V_{ex} \rangle$

At the percolation threshold, the product in Eq. (4) is also called the critical total average excluded volume [16]

$$\langle V_{ex} \rangle \equiv n_c \langle v_{ex} \rangle = B_c . \quad (8)$$

Figure 4(a) shows $\langle V_{ex} \rangle$ as a function of prism aspect ratio for all biaxial and some triaxial prisms investigated. Balberg [19], Haan and Zwanzig [12], and Balberg *et al.* [15] show that in 3D soft-core percolation $\langle V_{ex} \rangle = 2.8$ for spheres and parallel-aligned objects of any convex shape, $\langle V_{ex} \rangle = 0.7$ for orthogonally aligned (macroscopically isotropic) widthless sticks, and intermediate, $\langle V_{ex} \rangle \approx 1.4$ for highly elongated randomly oriented cylinders with hemispherical caps. Our results of $1.3 < \langle V_{ex} \rangle < 2.79$, for randomly oriented biaxial prisms, fall within Balberg's [19] bounds.

In the extreme oblate biaxial prism limit our simulations yield

$$\langle V_{ex} \rangle \approx 2.3 \quad \text{(extreme oblate prism limit)}. \quad (9)$$

This result is in close agreement with studies of similar object shapes [Fig. 4(a)] such as 2D polygons [4] and 2D ellipses [17] placed in a 3D system where $2.22 \leqslant \langle V_{ex} \rangle \leqslant 2.30$ and $\langle V_{ex} \rangle = 2.2$, respectively (our definition of $\langle V_{ex} \rangle$ is based on a unit volume bounding box and thus already normalized). The 2D shapes may be viewed as the extreme oblate limit of 3D objects. Garboczi *et al.* [14] report $\langle V_{ex} \rangle = 3.0$ for randomly oriented oblate rotational (biaxial) ellipsoids, a value higher than ours and above the upper bound of 2.8 suggested by Balberg [19]. This discrepancy has been noted by Garboczi *et al.* [14], Huseby *et al.* [4], and de Dreuzy *et al.* [17]. Results presented in Sec. V also suggest that for rotational ellipsoids values of $\langle V_{ex} \rangle$ are lower and possibly equal to values for biaxial prisms.

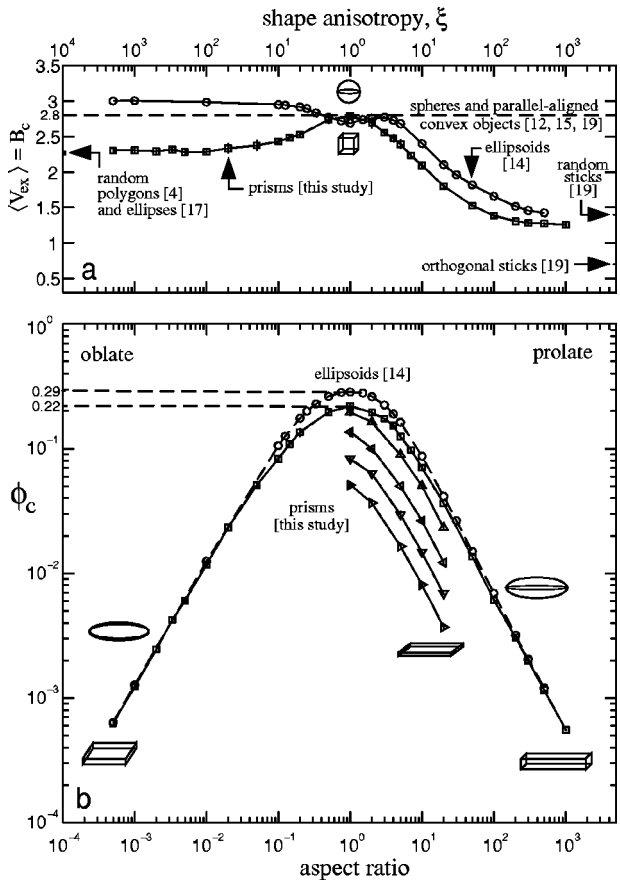

FIG. 4. Critical total average excluded volume $\langle V_{ex} \rangle$ [panel(a) and critical volume fraction ϕ_c [panel (b) at the percolation threshold versus aspect ratio (and shape anisotropy ξ) for biaxial (squares) and triaxial (triangles) prisms (this paper) and rotational (biaxial) ellipsoids (circles, from [14]). Short-over-medium axis aspect ratios for triaxial prisms are 1/2 (upward-pointing triangle), 1/5 (leftward-pointing triangle), 1/10 (downward-pointing triangle), and 1/20 (rightward-pointing triangle). Long-over-medium axis aspect ratios are as indicated by the figure axis. Error bars for prisms indicate 95% confidence intervals.

For an extreme prolate biaxial prism of aspect ratio 1000:1 we observe

$$\langle V_{ex} \rangle \approx 1.3 \quad \text{(extreme prolate prism limit)} \quad (10)$$

[Fig. 4(a)]. Balberg [19] finds $\langle V_{ex} \rangle \approx 1.4$ for extremely elongated randomly oriented cylinders with hemispherical caps.

In general, maximum values of $\langle V_{ex} \rangle = 2.8$ occur for parallel-aligned objects of any convex shape [6,15], where the most equant shape possible, a sphere, is always aligned. Therefore, it may be expected that we find a maximum of

$$\langle V_{ex} \rangle \approx 2.79 \quad \text{(cubes)} \quad (11)$$

for the most equant prism shape, a cube [Fig. 4(a)], where the effect of randomness in orientation is at a minimum.

It has been argued [14,19,20,28] that the total average excluded volume $\langle V_{ex}\rangle$ is not a true invariant but may be viewed as an approximate invariant that is less sensitive to object shapes than ϕ_c. Our results confirm this reduced variability of $\langle V_{ex}\rangle$ as a function of shape aspect ratio (Fig. 4). At the same time, $\langle V_{ex}\rangle \approx 2.3$ shows good agreement between extremely oblate prisms, 2D polygons, and 2D ellipses, where the 2D shapes are the extreme oblate 3D limits. Similarly, $\langle V_{ex}\rangle \approx 1.3$ applies to extremely prolate prisms, ellipsoids, and rods (hemispherically capped cylinders).

VI. CRITICAL VOLUME FRACTION ϕ_c

Figure 4b shows ϕ_c as a function of aspect ratio for randomly oriented soft-core biaxial (squares) and triaxial (triangles) prisms. The maximum value of ϕ_c is reached for the most equant prism shape (cube with aspect ratio 1:1:1). Increasing shape anisotropies due to flattening or elongation decrease ϕ_c for biaxial prisms. The combined effect of flattening and elongation of triaxial prisms decreases ϕ_c further [Fig. 4(b)]. The larger the shape anisotropy of an object the greater its normalized excluded volume, $\langle \overline{v_{ex}} \rangle$ (Fig. 3) and probability of overlap. As a result, percolation occurs at lower number densities n_c. Lower n_c values for different object shapes result in reduced ϕ_c in Eq. (1), where differences in object volume have already been accounted for by the volume normalization in $\langle \overline{v_{ex}} \rangle$.

The circles in Fig. 4(b) are results from Garboczi *et al.* [14] for randomly oriented soft-core rotational (biaxial) ellipsoids. Curves of ϕ_c, as a function of aspect ratio, for ellipsoids and prisms have similar shapes but are offset for the most equant shapes and converge in the extreme oblate and prolate limits. The offset between the curves for prisms and ellipsoids may be a function of the ratio

$$R = \frac{\langle \overline{v_{ex}} \rangle_e}{\langle \overline{v_{ex}} \rangle_p} \tag{12}$$

for a given aspect ratio. If we assume that for a given aspect ratio

$$\langle V_{ex}\rangle_p \cong \langle V_{ex}\rangle_e , \tag{13}$$

then by Eq. (8)

$$n_p \langle v_{ex}\rangle_p = n_e \langle v_{ex}\rangle_e , \tag{14}$$

where here and in all following equations the subscripts e and p denote parameters for ellipsoids and prisms, respectively. All parameters are defined as before with n_p, n_e, $\langle V_{ex}\rangle_p$, $\langle V_{ex}\rangle_e$, ϕ_p, and ϕ_e being critical values at the percolation threshold. Substituting Eq. (1) into Eq. (14) yields

$$\frac{\langle v_{ex}\rangle_p}{V_p} \ln(1-\phi_p) = \frac{\langle v_{ex}\rangle_e}{V_e} \ln(1-\phi_e). \tag{15}$$

Applying Eq. (6) to the appropriate terms for prisms and ellipsoids in Eq. (15), then substituting Eq. (12), and rearranging yields the critical prism volume fraction

$$\phi_p = 1-(1-\phi_e)^R. \tag{16}$$

In the extreme oblate and prolate limits, the ratio in the exponent R approaches one (Fig. 3) and thus Eq. (16) reduces to $\phi_p = \phi_e$ as expected from Fig. 4(b). For the most equant shape (cube and sphere) the ratio is at its minimum of

$$R = \frac{8.00}{10.56} = 0.758, \tag{17}$$

indicating that the normalized average excluded volume for a sphere is 75.8% of the one for a cube. The larger excluded volume of a cube with respect to a sphere causes percolation at a lower volume fraction for cubes than for spheres. With the result from Eq. (17) and $\phi_e = 0.2896$ [10,11,13,14] for spheres Eq. (16) yields $\phi_p = 0.23$ for cubes, agreeing, to within the uncertainty, with our numerical results of $\phi_p = 0.22$. The agreement between results from Eq. (16) and numerical results [Fig. 4(b)] for the most equant shapes as well as for the extreme aspect ratio limits suggest that $\langle V_{ex}\rangle$ may be invariant for a given aspect ratio as postulated by Eq. (13). Thus, the curves in Fig. 4(a) are expected to converge for a given aspect ratio, possibly to $\langle V_{ex}\rangle_p$ for prisms which agrees with results for 2D objects [Fig. 4(a)].

In the extreme oblate and prolate limits, the exponents of the power-law relating aspect ratio (or shape anisotropy ξ) to ϕ_c are close to ± 1 [line of slope ± 1 in Fig. 4(b)], indicating a linear relationship. Indeed, because ϕ_c is comparable for ellipsoids and prisms for $\xi > 50$, in this limit, the linear relationships

$$\phi_c = \begin{cases} 0.6/\xi & \text{(prolate)} \\ 1.27/\xi & \text{(oblate)} \end{cases} \tag{18}$$

hold true for both biaxial prisms (this paper) and rotational ellipsoids [14], where the shape anisotropy ξ is the ratio of large-over-small axis for both prolate and oblate objects.

VII. SUMMARY

The percolation system of randomly oriented 3D soft-core prisms serves as a link combining characteristics between other systems such as 3D ellipsoids, 3D cylinders with hemispherical caps (rods), 2D polygons, and 2D ellipses. All objects are randomly oriented and randomly placed in the 3D continuum. The 2D shapes are the extreme oblate limit of 3D objects.

Percolation parameters such as the critical volume fraction ϕ_c, the critical total average excluded volume $\langle V_{ex}\rangle \equiv n_c \langle v_{ex}\rangle$, or equivalently the average number of bonds per object, $B_c = n_c \langle v_{ex}\rangle$, can be related in most of the abovementioned systems. Here, in the extreme oblate and prolate limits $B_c \approx 2.3$ and $B_c \approx 1.3$, respectively. The minimum shape anisotropy of prisms is matched for cubes where $B_c = 2.79$ reaches the prism maximum, close to $B_c = 2.8$ for spheres.

With respect to biaxial prisms, triaxial prisms have increased normalized average excluded volumes $\langle \overline{v_{ex}} \rangle$ due to increased shape anisotropies. As a result, ϕ_c for triaxial prisms is lower than ϕ_c for biaxial prisms.

An offset in the critical object volume fraction ϕ_c occurs between prisms and ellipsoids with low shape anisotropy. This offset appears to be a function of the ratio of the normalized average excluded volume for ellipsoids $\langle \overline{v_{ex}} \rangle_e$ over $\langle \overline{v_{ex}} \rangle_p$ for prisms. Prisms and ellipsoids yield converging values for $\langle \overline{v_{ex}} \rangle$, and thus also for ϕ_c, in the extreme oblate and prolate limits. In these limits both parameters exhibit a linear relationship with respect to aspect ratio.

ACKNOWLEDGMENTS

Comments by Edward Garboczi were greatly appreciated. Katharine V. Cashman is thanked for discussions, support, and motivation. We thank Sean Fremouw for his contributions to the initial percolation code and John Conery for providing computer resources and computational advice. Charley Paffenbarger is also thanked for providing computer resources and efficient system administration. This work was supported by the Petroleum Research Fund, administered by the Chemical Society of America and by the National Science Foundation Grant No. EAR 0003303. Visualizations of simulations were made using Geomview.

[1] D. Bentz and E. Garboczi, Cem. Concr. Res. **21**, 325 (1991).
[2] W. Borchard and M. Lechtenfeld, Mater. Res. Innovations **4**, 381 (2001).
[3] M. Saar, M. Manga, K. Cashman, and S. Fremouw, Earth Planet. Sci. Lett. **187**, 367 (2001).
[4] O. Huseby, J.-F. Thovert, and P.M. Adler, J. Phys. A **30**, 1415 (1997).
[5] M. Saar and M. Manga, Geophys. Res. Lett. **26**, 111 (1999).
[6] A. Skal and B. Shklovskii, Fiz. Tekh. Poluprov. **7**, 1589 (1973) [Sov. Phys. Semicond. **7**, 1058 (1974)].
[7] A. Fizazi, J. Moulton, K. Pakbaz, S. Rughooputh, P. Smith, and A. Heeger, Phys. Rev. Lett. **64**, 2180 (1990).
[8] J. Yi and G. Choi, J. Electroceram. **3**, 361 (1999).
[9] D. Turcotte, Rep. Prog. Phys. **62**, 1377 (1999).
[10] K. Shante and S. Kirkpatrick, Adv. Phys. **20**, 325 (1971).
[11] G. Pike and C. Seager, Phys. Rev. B **10**, 1421 (1974).
[12] S. Haan and R. Zwanzig, J. Phys. A **10**, 1547 (1977).
[13] C. Lorenz and R. Ziff, J. Chem. Phys. **114**, 3659 (2001).
[14] E. Garboczi, K. Snyder, J. Douglas, and M. Thorpe, Phys. Rev. E **52**, 819 (1995).
[15] I. Balberg, N. Binenbaum, and N. Wagner, Phys. Rev. Lett. **52**, 1465 (1984).
[16] I. Balberg, C. Anderson, S. Alexander, and N. Wagner, Phys. Rev. B **30**, 3933 (1984).
[17] J.-R. de Dreuzy, P. Davy, and O. Bour, Phys. Rev. E **62**, 5948 (2001).
[18] L. Onsager, Ann. N.Y. Acad. Sci. **51**, 627 (1949).
[19] I. Balberg, Phys. Rev. B **31**, 4053 (1985).
[20] A. Drory, B. Berkowitz, G. Parisi, and I. Balberg, Phys. Rev. E **56**, 1379 (1997).
[21] E. Garboczi, M. Thorpe, M. DeVries, and A. Day, Phys. Rev. A **43**, 6473 (1991).
[22] I. Balberg, Phys. Rev. B **37**, 2391 (1988).
[23] D. Stauffer and A. Aharony, *Intrdoduction to Percolation Theory* (Taylor and Francis, London, 1992).
[24] A. Isihara, J. Chem. Phys. **18**, 1446 (1950).
[25] J. de la Torre, S. Harding, and B. Carrasco, Eur. Biophys. J. **28**, 119 (1999).
[26] A. Philipse, Langmuir **12**, 1127 (1996).
[27] L. Nichol, P. Jeffrey, and D. Winzor, J. Phys. Chem. **80**, 648 (1976).
[28] A. Drory, Phys. Rev. E **54**, 5992 (1996).